Supporting Information

Exploring the Triplet-to-Singlet Conversion Mechanism in Persistent Luminescence: Insights from a Host-Guest System

Fernando Teixeira Bueno[1], Tiago de Sousa Araújo Cassiano[1], Piotr de Silva[2], Pedro Henrique de Oliveira Neto[1,3] and Leonardo Evaristo de Sousa[21]

[1]*Institute of Physics, University of Brasília, Brasília-DF, 70910-900, DF, Brazil*

[2]*Department of Energy Conversion and Storage, Technical University of Denmark, Anker Engelunds Vej 301, 2800 Kongens Lyngby, Denmark*

[3]*International Center of Physics, Institute of Physics, University of Brasilia, Brazil*

S1. KINETIC MONTE CARLO

A. Morphology Model

ρ_{NPB}	ρ_{DCJTB}	ρ_{PMMA}	P_{NPB} (%)	P_{DCJTB} (%)	P_{PMMA} (%)	P_{dop} (%)	d_{avg} (Å)	$DCJTB_{sites}$ (%)
2.0	0.0	98.0	0.35	0.00	99.65	0.346	33.05	0.0
	0.2	97.8		0.05	99.61	0.394	31.65	12.1
	0.5	97.5		0.12	99.53	0.467	29.92	25.5
	0.8	97.2		0.19	99.46	0.539	28.51	35.4
	1.1	96.9		0.26	99.39	0.612	27.33	43.0
	1.4	96.6		0.34	99.31	0.686	26.32	49.0
	1.7	96.3		0.41	99.24	0.759	25.44	53.8
	2.0	96.0		0.48	99.17	0.833	24.66	58.7

TABLE S1. Donor concentration (ρ_{NPB}), acceptor concentration (ρ_{DCJTB}) and PMMA matrix concentration (ρ_{PMMA}) in molecular weight percentage (wt%). Contribution to sample composition by NPB (P_{NPB}), DCJTB (P_{DCJTB}) and PMMA (P_{PMMA}), according to equation S3. Probability of a dopant to be found within the sample (P_{dop}), average intermolecular distance between dopants (d_{avg}) and the percentage of sites containing acceptor molecules ($DCJTB_{sites}$) are shown in the last three columns, respectively.

In order to perform KMC simulations, the system's morphology needs to be obtained in terms of the number of each molecule and how they are spread across a lattice. To that end, we took the experimental concentrations of each dopant (NPB and DCJTB) within a PMMA matrix. The experimental data kept the concentration of NPB, ρ_{NPB}, constant at 2.0 wt% while varying the acceptor's concentration, ρ_{DCJTB}, between 0.0 wt% and 2.000 wt%. Assuming the increase of acceptor concentration meant a reduction of PMMA concentration while not altering donor concentration, we were able to calculate the number of molecules in the system for each acceptor concentration using

$$N_i = \frac{\rho_i N_A M_{total}}{M_i}, \tag{S1}$$

where N_i is the number of each molecule, N_A is Avogadro's number, ρ_i is the concentration in wt%, M_{total} is the sample's total mass and M_i is its molecular weight. Thus, the total number of

molecules is,

$$N_{total} = \sum N_i = N_A M_{total} \sum \frac{\rho_i}{M_i} \tag{S2}$$

The probability of finding a certain molecule is simply given by the ratio of the number of said molecule and the sum of all molecules,

$$P_i = \frac{\rho i}{M_i \sum \frac{\rho_i}{M_i}} \tag{S3}$$

Our KMC model consists of a cubic lattice of $50 \times 50 \times 50$ sites that only accounts for dopants in its sites, with an average intermolecular distance that varies according to concentration due to the different number of acceptor molecules. To obtain the intermolecular distance between donor and acceptor molecules we calculate the probability of finding one of the dopants within the PMMA matrix as

$$P_{dop} = \frac{P_{NPB} + P_{DCJTB}}{P_{NPB} + P_{DCJTB} + P_{PMMA}}, \tag{S4}$$

which can be interpreted as the percentage of dopants in the system. With that in mind, the intermolecular distance between dopants, d_{avg}, was calculated as

$$d_{avg} = d_0 \sqrt[3]{\frac{1}{P_{dopants}}} \tag{S5}$$

in which d_0 is a estimated intermolecular distance between all molecules, including the PMMA matrix. Considering $d_0 = 5$ Å, we were able to calculate the average intermolecular distance and the relative percentage of materials present in the lattice's sites. The parameters described above are shown in Table S1.

B. Medium Polarity

Experimental data suggests strong sample polarization as a result of increasing DCJTB dopant concentration[1,2]. The same phenomenon is observed in films made of a similar molecule: 4-(Dicyanomethylene)-2-methyl-6-julolidyl-9-enyl-4H-pyran (DCM2). As a result, the emission spectra of these molecules undergo redshift as their concentration increases, similarly to what is observed in solution when solvent polarity increases. As such, this sample polarization effect can be modeled by considering the static dielectric constant of the film to increase with the dopant's concentration. To quantify this effect, we rely on the observation that emission energies are affected by solvent polarity as follows[3]:

$$E_{sol} = E_{vac} - \chi \left(\frac{\varepsilon - 1}{\varepsilon + 1} \right) \tag{S6}$$

where E_{sol} and E_{vac} are the emission energies in solution and vacuum; χ is the solvent susceptibility and ε is the solvent's static dielectric constant.

Solvent susceptibility and E_{vac} can be determined by fitting experimental emission peaks measured in different solvents with Equation S6. Once that is done, experimental emission peaks measured in films of varying dopant concentration can be used to infer the ε values of each film. Finally, the dielectric constant values obtained this way can be fitted as a function of dopant concentration providing ε values for any desired concentration. Results of this procedure are shown in Table S2.

NPB Conc. (wt%)	DCJTB Conc. (wt%)	ε	n
2.0	0.0	2.45	1.485
	0.2	2.88	
	0.5	3.52	
	0.8	4.16	
	1.1	4.80	
	1.4	5.44	
	1.7	6.08	
	2.0	6.72	

TABLE S2. Interpolated dielectric constants corresponding to different acceptor concentrations.

S2. ELECTRONIC STRUCTURE RESULTS

A. Comparing Optical Properties

Molecule	Transition	Medium	ε	n	F_{max}^{calc} (nm)	F_{max}^{exp} (nm)
NPB	$S_0 \rightarrow S_1$	Thin film	3.000	1.785	336	343[4–6]
	$S_1 \rightarrow S_0$	$[PMMA:NPB]_{sc}$	3.000	1.485	440	425[7,8]
		$[TCTA:NPB]_{sc}$	3.035	1.718	441	440[7]
		$[TCTA:NPB]_{evap}$	3.035	1.718	441	430[7]
	$T_1 \rightarrow S_0$	$[PMMA:NPB]_{sc}$	3.000	1.485	603	540[7],550[8]
		$[TCTA:NPB]_{sc}$	3.035	1.718	585	540[7]
		$[TCTA:NPB]_{evap}$	3.035	1.718	585	540[7]
DCJTB	$S_1 \rightarrow S_0$	C_6H_6	2.270	1.490	556	563[1,2]
		$CHCl_3$	4.810	1.446	572	595[1]
		C_2H_5OH	24.300	1.361	608	645[1]
		$DMSO, (CH_3)_2S:O$	46.700	1.386	615	615[8],666[2]
	$T_1 \rightarrow S_0$	$PMMA$	3.000	1.485	779	-

TABLE S3. Calculated (F_{max}^{calc}) and experimental (F_{max}^{exp}) photoluminescence peaks for NPB and DCJTB in different media. Media's dielectric constants (ε) and refractive indices (n) are displayed.

B. DCJTB Thin Films

Ref. 2 reports on AlQ_3 films doped with three concentrations of DCJTB: 0.8 wt%, 1.5 wt% and 3.0 wt%. Using Table S2, we can interpolate the dielectric constants for each of those films. We then use those values for our simulated spectra. Results are shown in Table S4. The interpolation of dielectric constants and their use in simulating the corresponding spectra reproduce the experimental peaks within reasonable agreement, with a peak to peak difference no higher than 0.15 eV.

Molecule	Transition	Concentration (wt%)	ε^{calc}	F_{max}^{exp} (nm)	F_{max}^{calc} (nm)
DCJTB		0.8	4.16	606	566
		1.5	5.64	613	577
		3.0	8.84	635	592

TABLE S4. Experimental (F_{max}^{exp}) and simulated (F_{max}^{calc}) fluorescence peaks for AlQ_3 thin films doped with DCJTB in different concentrations. Estimated dielectric constants (ε^{calc}) are shown. Experimental data taken from Ref. 2

C. NPB's Phosphorescence Spectra

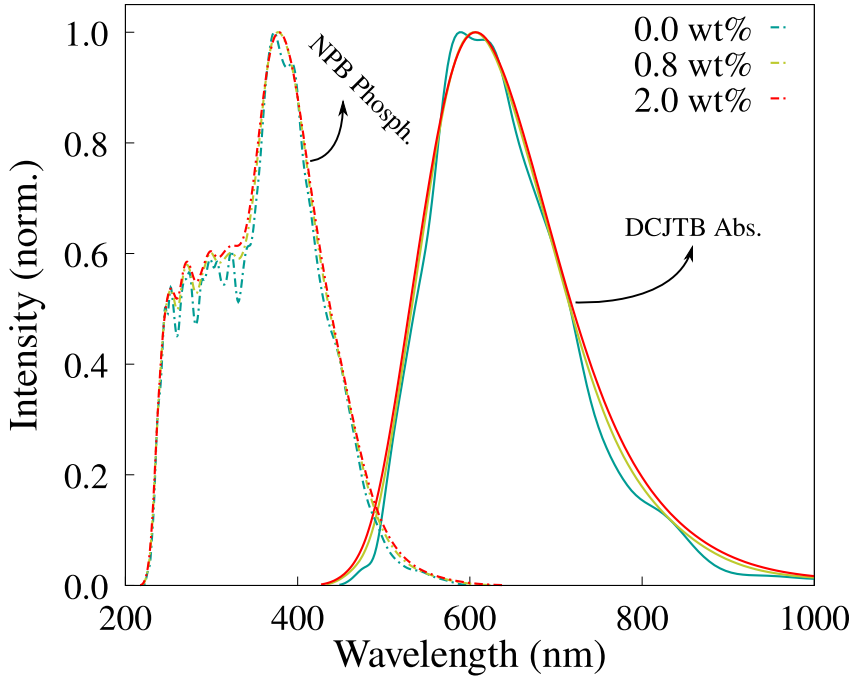

FIG. S1. Phosphorescence spectra for NPB (dashed lines) computed with dielectric constants associated with three different concentrations of DCJTB, 0 wt%, 0.8 wt% and 2.0 wt%. The full lines display the DCJTB absorption spectra for the corresponding concentrations.

D. Energy Levels Diagrams

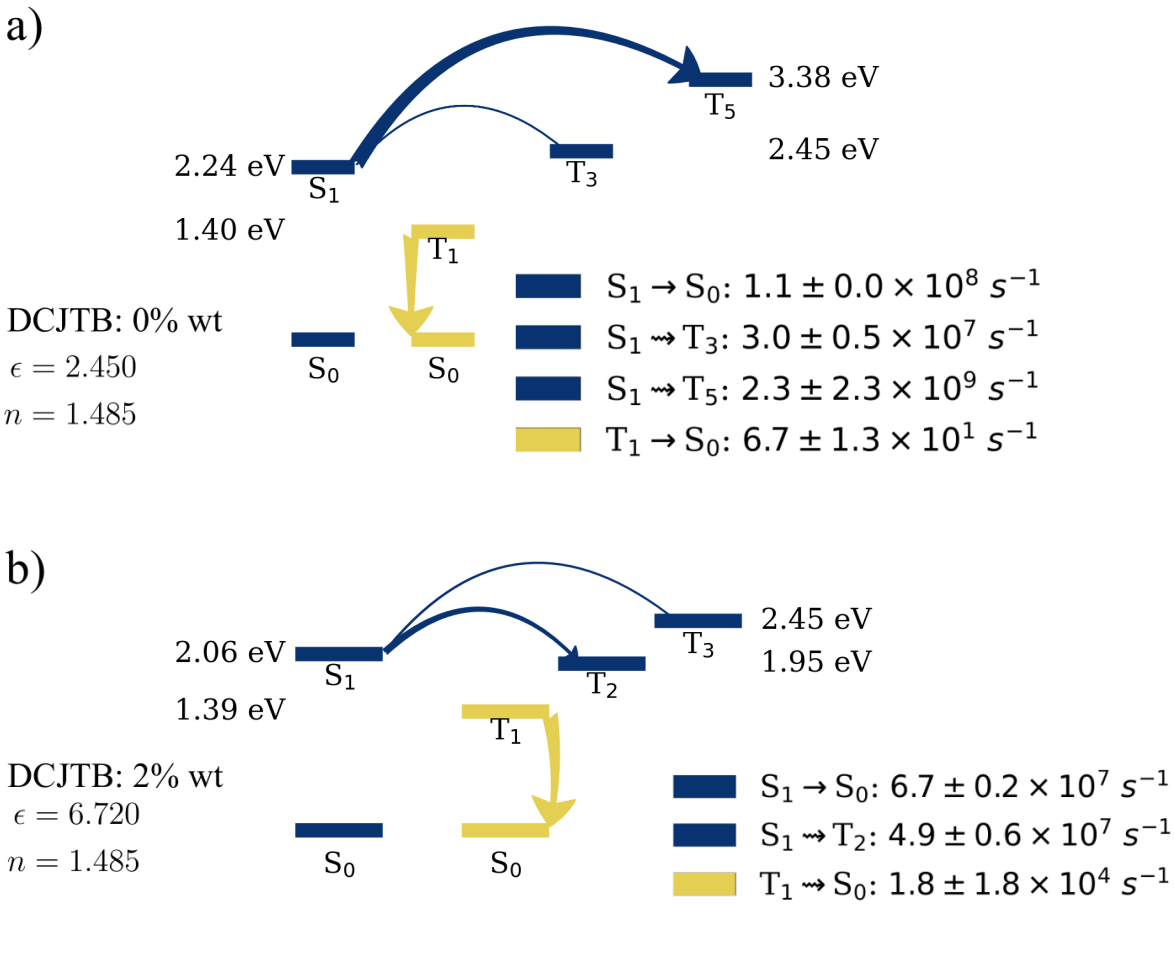

FIG. S2. Energy level diagram for DCJTB with (a) 0 wt% DCJTB concentration ($\varepsilon = 2.450$) and (b) 2 wt% concentration ($\varepsilon = 6.720$). Here, energy levels are computed as ensemble averages.

E. Average Spin-Orbit Couplings

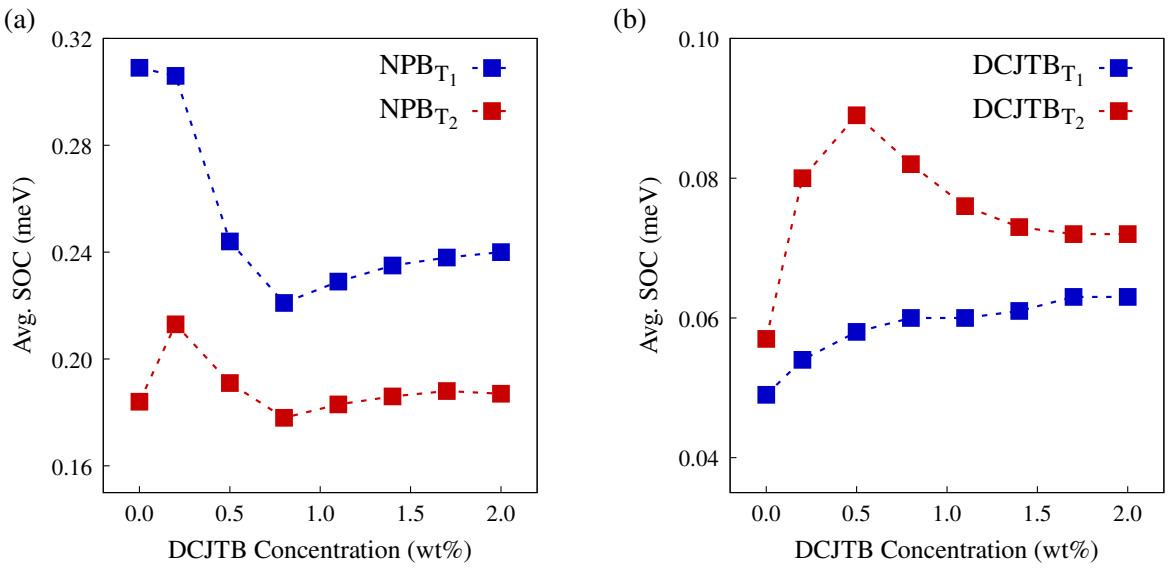

FIG. S3. Average spin-orbit coupling between the triplet states, T_1 (in blue) and T_2 (in red), and the first excited, S_1, for NPB (a) and DCJTB (b) taken from the first excited state ensemble for both molecules.

F. Average Emission Times

DCJTB Conc. (wt%)	Average fluorescence time (s)	
	Prompt Fluorescence	Afterglow
0.2	1.07×10^{-8}	7.26×10^{-1}
0.5	9.21×10^{-8}	7.19×10^{-1}
0.8	9.30×10^{-8}	6.92×10^{-1}
1.1	9.31×10^{-8}	6.66×10^{-1}
1.4	9.38×10^{-8}	6.66×10^{-1}
1.7	9.46×10^{-8}	6.84×10^{-1}
2.0	9.52×10^{-8}	7.13×10^{-1}

TABLE S5. Average fluorescence time for excitons that fluoresced in DCJTB in the different time scales it occurs, prompt and delayed (afterglow).

REFERENCES

[1]V. Bulović, A. Shoustikov, M. Baldo, E. Bose, V. Kozlov, M. Thompson, and S. Forrest, "Bright, saturated, red-to-yellow organic light-emitting devices based on polarization-induced spectral shifts," Chemical Physics Letters **287**, 455–460 (1998).

[2]D. Xu, Z. Deng, Y. Xu, J. Xiao, and C. Liang, "Bright red-to-yellow organic light-emitting devices based on polarization-induced spectral shifts and broadening," Displays **26**, 185–189 (2005).

[3]L. E. de Sousa and P. de Silva, "Photophysics of solvated molecules: Computational protocol combining nuclear ensemble and nonequilibrium state-specific solvation methods," The Journal of Physical Chemistry A **127**, 8200–8208 (2023).

[4]H. Mattoussi, H. Murata, C. D. Merritt, Y. Iizumi, J. Kido, and Z. H. Kafafi, "Photoluminescence quantum yield of pure and molecularly doped organic solid films," Journal of Applied Physics **86**, 2642–2650 (1999).

[5]D.-S. Leem, H.-D. Park, J.-W. Kang, J.-H. Lee, J. W. Kim, and J.-J. Kim, "Low driving voltage and high stability organic light-emitting diodes with rhenium oxide-doped hole transporting layer," Applied Physics Letters **91**, 011113 (2007).

[6]J. C. Costa, A. Mendes, and L. M. Santos, "Thin film deposition of organic hole transporting materials: optical, thermodynamic and morphological properties of naphthyl-substituted benzidines," Journal of Materials Science **53**, 12974–12987 (2018).

[7]C. Salas Redondo, P. Kleine, K. Roszeitis, T. Achenbach, M. Kroll, M. Thomschke, and S. Reineke, "Interplay of fluorescence and phosphorescence in organic biluminescent emitters," The Journal of Physical Chemistry C **121**, 14946–14953 (2017).

[8]A. Kirch, M. Gmelch, and S. Reineke, "Simultaneous singlet–singlet and triplet–singlet forster resonance energy transfer from a single donor material," The journal of physical chemistry letters **10**, 310–315 (2019).